Co-published by
Institute of Fluid-Flow Machinery
Polish Academy of Sciences
Committee on Thermodynamics and Combustion
Polish Academy of Sciences

http://www.imp.gda.pl/archives-of-thermodynamics/

An alternative formulation of the method of weighted residuals for the approximate solving of heat conduction problems

Jan Taler[a*], Dawid Taler[b]

[a]Cracow University of Technology, Faculty of Environmental Engineering and Energy, Department of Energy, 31-864 Cracow, Poland
[b]Cracow University of Technology, Faculty of Environmental Engineering and Energy, Department of Thermal Processes, Air Protection and Waste Utitilisation, 31-155 Cracow, Poland
*Corresponding author email: jan.taler@pk.edu.pl

Received: 27.01.2026; accepted: 19.02.2026

Abstract

An alternative formulation of the method of weighted residuals for Fourier's law of heat conduction is presented. In one-dimensional heat conduction, when the weighting factor equals unity and the heat-penetration-depth concept is used, the method reduces to the heat flux integral method. The paper also presents a comparison of the proposed heat flux integral method with the classic heat balance integral method developed by T.R. Goodman. In the heat balance integral method, the transient heat conduction equation is integrated with respect to the spatial coordinate, whereas in the heat flux integral method, Fourier's law is integrated over the spatial coordinate. The advantage of the heat flux integral method over the heat balance integral method is the greater accuracy, especially in bodies whose thermal conductivity depends on temperature or position. The greater accuracy of the proposed method is illustrated by the determination of the transient temperature distribution in a plate with temperature-dependent thermal conductivity. Additionally, for a straight fin with temperature-dependent thermal conductivity, the heat flux integral method provides greater accuracy in determining temperature and fin efficiency than the heat balance integral method. The temperature distribution in the plate and fin, as well as the fin efficiency, were also determined using the finite volume method to assess the accuracy of the heat flux integral method and heat balance integral method.

Keywords: Heat balance integral method; Heat flux integral method; Nonlinear heat conduction; Fin with variable thermal conductivity; Transient nonlinear heat conduction in a plate

Vol. 47(2026), No. 1, 25–41; doi: 10.24425/ather.2026.158663

Cite this manuscript as: Taler, J., & Taler, D. (2026). An alternative formulation of the method of weighted residuals for the approximate solving of heat conduction problems. *Archives of Thermodynamics*, 47(1), 25−41.

1. Introduction

A method of weighted residuals (MWR) is an approximate analytical method widely used to solve boundary and initial-boundary problems in thermal engineering. The popularity of the MWR stems from the simplicity and high accuracy of the analytical solutions obtained using this method, as well as the moderate effort required to calculate temperature values [1].

The MWR and its application to calculating temperature fields in boiler components are presented in [2]. Two-dimensional steady-state temperature and stress distributions in the tubes of the membrane walls of large steam boilers were determined. Using the MWR, transient temperature and stress distributions in pipelines, boiler drums and steam superheaters' headers were calculated [2]. In most cases, the solutions obtained not only illustrate the application of MWR but are also of great importance for industrial practice.

The MWR is an effective tool for solving nonlinear ordinary and partial differential equations, thanks to its simplicity and high accuracy. Hatami [3] demonstrated that MWRs, such as

Nomenclature

A – area, m^2
a, b, c – constants
$a_1, \ldots, a_n$ – unknown coefficients in the function approximating the temperature distribution
c – specific heat capacity, J/(kg·K)
C – constant
$C_1, \ldots, C_7$ – constants
$e_{\theta,i}$ – temperature difference $e_{\theta,i} = \theta_{i,num} - \theta_{i,app}$, $i = 1, \ldots, n$ between temperature values $\theta_{i,num}$ calculated by the numerical method and temperature $\theta_{i,app}$ calculated by HFIM or HBIM, K
$e_{\theta,\max}$ – maximum temperature difference between the temperature values $\theta_{i,num}$ calculated numerically by the method of lines, and the temperature $\theta_{i,app}$ calculated by the approximate analytical method HFIM or HBIM, K
$\bar{e}_\theta$ – mean-square temperature difference, K
Fo – Fourier number, Fo = $\alpha_0 \cdot t/L^2$
Fo$_1$ – Fourier number at the end of the first heat penetration phase, Fo$_1$ = $\alpha_0 \cdot t_1/L^2$
g, f, e – coefficients
H – heat transfer coefficient (HTC), W/(m^2·K)
k – thermal conductivity, W/(m·K)
K – dimensionless thermal conductivity,
L – plate thickness or fin height, m
m – power exponent in the heat conduction equation; $m = 1$ for cylindrical wall and $m = 2$ for spherical wall
n – number of nodes in the FVM grid
N – fin parameter, $N^2 = 2hL^2/[k(T_f)w]$
$\dot{q}$ – heat flux, W/m^2
$\dot{q}_{in}$ – heat flux at the inner surface, W/m^2
$\dot{q}_v$ – heat transfer rate per unit volume, W/m^3
$\dot{\mathbf{q}}$ – heat flux vector, W/m^2
$\tilde{q}$ – approximate solution for heat flux, W/m^2
r_{in} – inner radius, m
r_{out} – outer radius, m
R – radius, m
t – time, s
t_1 – the time after which the first phase of heat penetration ends, s
T – temperature, °C
T_b – fin base temperature, °C
T_f – fluid temperature, °C
T_s – slab surface temperature, °C
T_0 – initial temperature, °C
W – fin thickness, m
W_i – weighting factor
$\mathbf{W_i}$ – vector weighting factor
x, y, z – Cartesian coordinates, m
X – dimensionless x coordinate, $X = x/L$

Greek symbols

α – thermal diffusivity, m^2/s
$\alpha_C, \beta_C, \gamma_C, \alpha_c, \beta_c, \gamma_c$ – coefficients in a quadratic algebraic equation for determining the constant C
β, β_k – coefficients in functions determining the dependence of thermal conductivity on temperature
ΔX – dimensionless spatial step in FVM
∇ – gradient operator (nabla)
δ – heat penetration depth, m
δ^* – dimensionless heat penetration depth, $\delta^* = \delta/L$
Γ – boundary of the domain Ω
ε – constant in the function describing changes in the thermal conductivity as a function of temperature
η – fin efficiency
θ – dimensionless fin temperature, $\theta = (T - T_f)/(T_b - T_f)$
θ – dimensionless plate temperature, $\theta = (T - T_0)/(T_s - T_0)$
ρ – density, kg/m^3
Ω – domain with the boundary Γ

Subscripts and Superscripts

$\bar{}$ – mean
$\sim$ – approximate
$*$ – dimensionless
b – fin base
f – fluid temperature
i – node number or the weighting factor
in – inner surface
s – surface
out – outer surface
v – volume heat source
0 – at the initial state
I – the first phase of heat penetration
II – the second phase of heat penetration

Abbreviations and Acronyms

FVM – finite volume method
HBIM – heat balance integral method
HFIM – heat flux integral method
HTC – heat transfer coefficient
MWR – method of weighted residuals

collocation, Galerkin, Rayleigh–Ritz and least-squares methods, yield satisfactory results when solving numerous linear and nonlinear problems in heat transfer, nanotechnology and medicine. MRWs constitute a large group of methods, alongside other approximate analytical methods and analytical-numerical methods for solving ordinary and partial differential equations [4]. Ganji et al. [5] applied approximate analytical methods for direct nonlinear problems encountered in heat transfer. The homotopy perturbation, variational iteration and Adomian decomposition methods were used to solve nonlinear conduction-convection heat transfer problems, such as the cooling of a lumped system with a variable specific heat or heat transfer coefficient, and to determine the temperature distribution in a straight fin with a temperature-dependent conductivity. One of the most popular MWRs is the Galerkin method, which is now also used in the finite element method (FEM) [6]. Another widely used procedure is the method of moments, applied to approximate the distribution of substance concentration [7] or temperature in heat and mass transfer problems, as well as in electromagnetics [8]. A special case of MWR is the heat balance integral method (HBIM) proposed by Goodman [9]. An important and original feature of HBIM proposed by Goodman is the application of the boundary-layer thickness concept to transient heat conduction in solids. A counterpart of the thermal boundary layer thickness in convective heat transfer is the heat penetration depth in HBIM. The concept of boundary-layer thickness was originally pro-

posed by Pohlhausen [10] and von Kármán [11] to determine the distributions of velocity and temperature in a fluid near the channel surface. Due to the large velocity and temperature gradients normal to the channel surface, it is challenging to determine the correct distributions of fluid velocity and temperature near the channel wall, even with modern computational fluid dynamics (CFD) methods. A major advantage of HBIM, on the other hand, is the ability to determine the temperature of a solid near its surface for a very short heating or cooling time. Determining the temperature distribution in a solid at the beginning of a transient process using exact analytical methods can be subject to large errors due to the slow convergence of infinite series. Additionally, for numerical methods, it is necessary to integrate the heat conduction equation using very small time steps to achieve satisfactory accuracy in determining the temperature field near $t = 0$. The use of HBIM enables the determination of optimum fluid temperature changes at the beginning of heating pressurised structural elements over very small time intervals [12].

The HBIM method can also be used to solve problems of great practical importance, for example, to determine the optimal temperature changes in a fluid during the heating of a thick-walled pressure element with holes, accounting for the time-dependent pressure inside the component [13]. HBIM can also be used to approximate two-dimensional steady-state temperature distributions. The two-dimensional temperature distribution in tubes and flat bars (fins) connecting tubes in the tight waterwalls of the boiler combustion chamber was determined using HBIM in [14]. The temperature distribution in the boiler waterwall tube was also investigated in [15]. Examples of the application of HBIM to calculate transient temperature distributions in a half-space and a flat plate for various boundary conditions are presented in books [15,16]. HBIM is widely used for calculating temperature and thermal-stress fields in solids, as well as for thermal analysis of melting and solidification processes, and is continually being refined. Volkov and Li-Orlov [17] employed double integration of the heat conduction equation along the x-coordinate, as opposed to the single integration used in classical HBIM. Thanks to double integration, the accuracy of determining the transient temperature distribution in bodies with a temperature-dependent thermal conductivity has been increased. It should be emphasised that greater accuracy in the approximate solution for temperature-dependent thermal conductivity can also be achieved by using the Galerkin or moment method, with the concept of heat penetration depth used in HBIM. However, this requires slightly more mathematical transformations to determine the temperature distribution. The accuracy of HBIM, like all MWRs, depends on the accuracy of the solution obtained from the appropriate selection of the form of the function approximating the exact solution. Sitison and Edwards [18] applied the heat balance integral method to determine two-dimensional temperature distribution in cylindrical extruders. The problem was solved using a quasi-steady approximation in the crystal and HBIM in the melt.

Kumar and Rajeev [19] solved a time-fractional Stefan problem with a third-kind boundary condition and temperature-dependent thermal conductivity using HBIM. The conventional HBIM approach, utilising quadratic and exponential temperature profiles, was employed to determine an approximate temperature distribution.

A new approximation function for the temperature distribution using the Legendre wavelet was used by Chaurasiya et al. [20] in HBIM to solve a two-dimensional moving-boundary problem involving a moving phase-change material. They compared numerical results with the exact solution by transforming the analysed problem into a one-dimensional melting problem and found good agreement.

A review of the literature shows that the method of weighted residuals, in particular HBIM, is widely used in practice, both globally, where a single function approximates the temperature distribution across the entire analysed area, and in numerical methods such as FEM or hybrid FVM-FEM, in which MWR is applied locally, separately for each element. The abbreviation FVM stands for finite volume method, in which the energy conservation equation is satisfied for each finite volume with a node located inside it. In the case of heat conduction, MWR is formulated for the transient heat conduction equation, i.e. the energy conservation equation, which accounts for Fourier's law.

This paper presents a new formulation of MWR for solving heat conduction problems. MWR has been applied to Fourier's law, and not as in the classical MWR for the transient heat conduction equation, i.e. for the energy conservation equation.

The advantage of the new MWR formulation is its greater accuracy compared to the traditional MWR formulation, particularly when the weighting factor equals one. Both methods were compared using two examples: determining the transient temperature field in a plate with temperature-dependent thermal conductivity and determining the temperature and efficiency of a fin with temperature-dependent thermal conductivity. The new MWR formulation, with a weighting factor of 1, referred to as the heat flux integral method (HFIM), yields higher-accuracy solutions than the traditional MWR formulation (HBIM) in both cases.

The paper presents the following issues in sequence: characteristics of the classical MWR, a new formulation of MWR in heat conduction problems, determining the transient temperature of a flat wall with linearly dependent thermal conductivity using HBIM and HFIM, determining the temperature and efficiency of a fin with linearly dependent thermal conductivity using HBIM and HFIM, conclusions, future work, and, in the Appendix, two different approaches for determining one-dimensional steady-state temperature distributions.

The next section will provide a brief discussion of classical MWR, focusing on the integral heat balance method.

2. Classic MWRs in heat conduction problems

MWRs are widely used for approximate solutions to boundary and initial-boundary problems of heat conduction. The governing heat conduction equation is:

$$c(T)\rho(T)\frac{\partial T}{\partial t} = \nabla \cdot [k(T)\nabla T] + \dot{q}_v. \tag{1}$$

The boundary conditions and initial conditions are known. The initial condition is as follows:

$$T|_{t=0} = T_0(x,y,z). \quad (2)$$

The approximate solution $\tilde{T}$ of Eq. (1) satisfying the boundary conditions is sought in the form:

$$\tilde{T} = \tilde{T}[x,y,z,a_1(t),\ldots,a_n(t),t]. \quad (3)$$

The parameters $a_1(t)$, …, $a_n(t)$ are determined using the WRM method from the following system of equations:

$$\int_\Omega \left\{c(\tilde{T})\rho(\tilde{T})\frac{\partial \tilde{T}}{\partial t} - \nabla\cdot\left[k(\tilde{T})\nabla\tilde{T}\right] - \dot{q}_v\right\} W_i dV = 0, \quad i = 1,\ldots,n. \quad (4)$$

The initial values of parameters $a_1(0)$,…, $a_n(0)$ are determined from the solution of the following system of algebraic equations:

$$\int_\Omega \{\tilde{T}[x,y,z,a_1(0),\ldots,a_n(0)] - T_0(x,y,z)\}\ W_i dV = 0, \quad i = 1,\ldots,n. \quad (5)$$

A system of ordinary differential equations or algebraic equations from which the unknown coefficients a_i are determined consists of n equations. In practical applications, the unknown parameters a_1,…, a_n are independent of time.

Depending on the weighting factor W_i, several MWRs [1] can be distinguished, such as the heat balance method, when $W_1 = 1$ and $W_i = 0$ for $i = 2, \ldots, n$; the moment method, when for one-dimensional problems $W_i = x^i$, $i = 0, \ldots, n$; the Galerkin method when $W_i = \partial\tilde{T}/\partial a_i$, $i = 1, \ldots, n$; the least squares method, the collocation method, and the subdomain method. The weighting factors should be simple, and their number small, as the work involved in deriving the analytical form of the function for calculating the temperature field is usually considerable. The simplest MRW is the heat balance method, in which the equation of transient heat conduction is integrated over volume, as the weighting factor is equal to unity:

$$\int_\Omega \left[c(\tilde{T})\rho(\tilde{T})\frac{\partial \tilde{T}}{\partial t} = \nabla\cdot\left[k(\tilde{T})\nabla\tilde{T}\right] + \dot{q}_v\right] dV = 0. \quad (6)$$

Green's theorem [21,22] was used to transform Eq. (6):

$$\int_\Omega \nabla\cdot\left[k(\tilde{T})\nabla\tilde{T}\right] dV = \int_\Gamma k(\tilde{T})\frac{\partial \tilde{T}}{\partial n}\, dA, \quad (7)$$

where Γ denotes the boundary of the domain Ω, and $\partial\tilde{T}/\partial n$ is the derivative in the direction normal to the surface of the analysed domain.

Substituting Eq.(7) into Eq.(6) gives:

$$\int_\Omega c(\tilde{T})\,\rho(\tilde{T})\frac{\partial \tilde{T}}{\partial t} dV = \int_\Gamma k(\tilde{T})\frac{\partial \tilde{T}}{\partial n} dA + \int_\Omega \dot{q}_v\, dV. \quad (8)$$

Analysis of Eq. (8) shows that in the case of temperature-dependent thermal conductivity, the accuracy of determining the temperature field is low, as thermal conductivity is calculated only at the temperature of the boundary of the analysed area.

If the temperature field is determined in a small cell, such as in FEM or the hybrid FVM-FEM method [23], Eq. (8) provides good accuracy, as the temperature difference inside the element is small. The FVM-FEM method is used in commercial programmes STAR-CCM+CFD [24] and ANSYS-FLUENT [25] for modelling heat transfer processes. When determining the temperature field in bodies with temperature- or position-dependent thermal conductivity and large dimensions without discretisation, it is better to use the Galerkin or moment method. This can be demonstrated by transforming Eq. (4), in which the weight factor differs from one. The following equality was used to transform Eq. (4):

$$W_i\nabla\cdot\left[k(\tilde{T})\nabla\tilde{T}\right] = \nabla\cdot\left[W_i k(\tilde{T})\nabla\tilde{T}\right] - \nabla W_i\cdot\left[k(\tilde{T})\nabla\tilde{T}\right]. \quad (9)$$

Considering Eq. (9) in Eq. (4) results in:

$$\int_\Omega \left\{c(\tilde{T})\rho(\tilde{T})\frac{\partial \tilde{T}}{\partial t}W_i - \nabla\cdot\left[W_i k(\tilde{T})\nabla\tilde{T}\right] + \nabla W_i\cdot\left[k(\tilde{T})\nabla\tilde{T}\right] - \dot{q}_v W_i\right\} dV = 0, \quad i = 1,\ldots,n. \quad (10)$$

The second term in Eq. (10) was transformed using Green's theorem:

$$\int_\Omega \nabla\cdot\left[W_i k(\tilde{T})\nabla\tilde{T}\right] dV = \int_\Gamma W_i k(\tilde{T})\nabla\tilde{T}\cdot\boldsymbol{n}\, dA. \quad (11)$$

Considering that:

$$\nabla\tilde{T}\cdot\boldsymbol{n} = \frac{\partial \tilde{T}}{\partial n}, \quad (12)$$

Eq. (10) can be written as:

$$\int_\Omega \left\{c(\tilde{T})\rho(\tilde{T})\frac{\partial \tilde{T}}{\partial t}W_i + \nabla W_i\cdot\left[k(\tilde{T})\nabla\tilde{T}\right] - \dot{q}_v W_i\right\} dV = \int_\Gamma W_i k(\tilde{T})\frac{\partial \tilde{T}}{\partial n} dA, \quad i = 1,\ldots,n. \quad (13)$$

Comparing Eq. (13) with Eq. (8), it can be seen that Eq. (13) is derived with the weight factor $W_i = W_i(x,y,z)$. There is a term:

$$\int_\Omega \nabla W_i\cdot\left[k(\tilde{T})\nabla\tilde{T}\right] dV, \quad (14)$$

taking into account the temperature-dependent thermal conductivity throughout the analysed domain Ω, and not only at the edge Γ of the domain Ω. This can also be seen in the example of MRW used to determine the one-dimensional heat conduction equation while utilising the concept of heat penetration depth $\delta(t)$, for which Eq. (13) takes the following form:

$$\int_0^\delta \left[c(\tilde{T})\rho(\tilde{T})\frac{\partial \tilde{T}}{\partial t}W_i + k(\tilde{T})\frac{\partial W_i}{\partial x}\frac{\partial \tilde{T}}{\partial x} - \dot{q}_v W_i\right] dx = W_i\, k(\tilde{T})\frac{\partial \tilde{T}}{\partial x}\Big|_{x=\delta} - W_i\, k(\tilde{T})\frac{\partial \tilde{T}}{\partial x}\Big|_{x=0}, \quad i = 1,\ldots,n, \quad (15)$$

where $W_i = W_i(x)$.

It should be noted that in Eq. (15), the temperature distribution is approximated by the function $\tilde{T} = \tilde{T}[x, \delta(t), a_2, \ldots, a_n]$, since $a_1 = \delta(t)$. Analysis of Eq. (15) reveals that the second term in the integral accounts for changes in thermal conductivity throughout the entire analysed domain, rather than just at the boundary, as is the case in classical HBIM [9], where there is only one weighting coefficient $W_1 = 1$.

For this reason, the method of moments or Galerkin's method gives better results for temperature or space-dependent thermal conductivity than HBIM given by Eq. (8). However, the method of moments and Galerkin's method involve more work in determining the coefficients $a_1, \ldots, a_n$.

3. Alternative formulation of MWRs in heat conduction problems

It was shown in Appendix that the steady-state temperature distribution in a solid can be determined using the equation of energy conservation or Fourier's law. Following the same line of thought, an alternative formulation of MWR for solving heat conduction problems based on Fourier's law has been proposed:

$$\int_\Omega \left[\tilde{\mathbf{q}} + k(\tilde{T})\nabla\tilde{T}\right]\cdot \mathbf{W_i} dV = 0, \qquad i = 1, \ldots, n, \tag{16}$$

where: $\dot{\mathbf{q}} = (\dot{q}_x, \dot{q}_y, \dot{q}_z)$ – heat flux vector, $\nabla T = (\partial T/\partial x, \partial T/\partial y, \partial T/\partial z)$ – gradient of T, and $\mathbf{W}_i = (W_{x,i}, W_{y,i}, W_{z,i})$ – weighting factor.

The heat flux vector $\tilde{\mathbf{q}}$ is determined from the energy conservation equation:

$$c(\tilde{T})\rho(\tilde{T})\frac{\partial \tilde{T}}{\partial t} = -\nabla\cdot\tilde{\mathbf{q}} + \dot{q}_v. \tag{17}$$

Equations (16) and (17) take the following form in the Cartesian coordinate system:

$$\int_\Omega \left\{\left[\tilde{q}_x + k(\tilde{T})\frac{\partial \tilde{T}}{\partial x}\right]W_{x,i} + \left[\tilde{q}_y + k(\tilde{T})\frac{\partial \tilde{T}}{\partial y}\right]W_{y,i} + \left[\tilde{q}_z + k(\tilde{T})\frac{\partial \tilde{T}}{\partial z}\right]W_{z,i}\right\} dxdydz = 0, \tag{18}$$

$$i = 1, \ldots, n,$$

$$c(\tilde{T})\rho(\tilde{T})\frac{\partial \tilde{T}}{\partial t} = -\frac{\partial \tilde{q}_x}{\partial x} - \frac{\partial \tilde{q}_y}{\partial y} - \frac{\partial \tilde{q}_z}{\partial z} + \dot{q}_v. \tag{19}$$

The components $\tilde{q}_x$, $\tilde{q}_y$, $\tilde{q}_z$ of heat flux are determined respectively from the energy conservation equation written in the following forms:

$$c(\tilde{T})\rho(\tilde{T})\frac{\partial \tilde{T}}{\partial t} = -\frac{\partial \tilde{q}_x}{\partial x} + \frac{\partial}{\partial y}\left[k(\tilde{T})\frac{\partial \tilde{T}}{\partial y}\right] + \frac{\partial}{\partial z}\left[k(\tilde{T})\frac{\partial \tilde{T}}{\partial z}\right] + \dot{q}_v, \tag{20}$$

$$c(\tilde{T})\rho(\tilde{T})\frac{\partial \tilde{T}}{\partial t} = \frac{\partial}{\partial x}\left[k(\tilde{T})\frac{\partial \tilde{T}}{\partial x}\right] - \frac{\partial \tilde{q}_y}{\partial y} + \frac{\partial}{\partial z}\left[k(\tilde{T})\frac{\partial \tilde{T}}{\partial z}\right] + \dot{q}_v, \tag{21}$$

$$c(\tilde{T})\rho(\tilde{T})\frac{\partial \tilde{T}}{\partial t} = \frac{\partial}{\partial x}\left[k(\tilde{T})\frac{\partial \tilde{T}}{\partial x}\right] + \frac{\partial}{\partial y}\left[k(\tilde{T})\frac{\partial \tilde{T}}{\partial y}\right] - \frac{\partial \tilde{q}_z}{\partial z} + \dot{q}_v. \tag{22}$$

After determining the derivative $\partial\tilde{q}_x/\partial x$ from Eq. (20) and then integrating it with respect to x, the following expression for calculation $\tilde{q}_x$ is obtained:

$$\tilde{q}_x = \int\left\{-c(\tilde{T})\rho(\tilde{T})\frac{\partial \tilde{T}}{\partial t} + \frac{\partial}{\partial y}\left[k(\tilde{T})\frac{\partial \tilde{T}}{\partial y}\right] + \frac{\partial}{\partial z}\left[k(\tilde{T})\frac{\partial \tilde{T}}{\partial z}\right] + \dot{q}_v\right\}dx + C_x. \tag{23}$$

The components $\tilde{q}_y$ and $\tilde{q}_z$ were determined in a similar manner:

$$\tilde{q}_y = \int\left\{-c(\tilde{T})\rho(\tilde{T})\frac{\partial \tilde{T}}{\partial t} + \frac{\partial}{\partial x}\left[k(\tilde{T})\frac{\partial \tilde{T}}{\partial x}\right] + \frac{\partial}{\partial z}\left[k(\tilde{T})\frac{\partial \tilde{T}}{\partial z}\right] + \dot{q}_v\right\}dy + C_y, \tag{24}$$

$$\tilde{q}_z = \int\left\{-c(\tilde{T})\rho(\tilde{T})\frac{\partial \tilde{T}}{\partial t} + \frac{\partial}{\partial x}\left[k(\tilde{T})\frac{\partial \tilde{T}}{\partial x}\right] + \frac{\partial}{\partial y}\left[k(\tilde{T})\frac{\partial \tilde{T}}{\partial y}\right] + \dot{q}_v\right\}dz + C_z. \tag{25}$$

The constants C_x, C_y, and C_z in Eqs. (23)−(25) are determined from boundary conditions. After substituting the heat flux components $\tilde{q}_x$, $\tilde{q}_y$ and $\tilde{q}_z$, defined by Eqs. (23)−(25) into Eq. (18), a system of n first-order ordinary equations for transient problems, from which the desired parameters appearing in the approximate solution $\tilde{T}(x, y, z, t)$ are determined. If a steady-state problem is considered, Eq. (18) yields a system of n algebraic equations, from which the unknown parameters appearing in the approximate solution are determined.

When determining a one-dimensional transient temperature field in the 1D-region $[x_1, x_2]$, the system of Eq. (16) takes the following form:

$$\int_{x_1}^{x_2}\left[\tilde{q} + k(\tilde{T})\frac{\partial \tilde{T}}{\partial x}\right]W_i dx = 0, \quad i = 1, \ldots, n. \tag{26}$$

The heat flux $\tilde{q}$ in Eq.(26) is determined from Eq.(23), which in this case takes the following form:

$$\tilde{q} = \int\left[-c(\tilde{T})\rho(\tilde{T})\frac{\partial \tilde{T}}{\partial t} + \dot{q}_v\right]dx + C_x, \tag{27}$$

where $\tilde{q} = \tilde{q}_x$ is the x-component of the vector $\tilde{\mathbf{q}}$.

If the concept of heat penetration depth $a_1 = \delta(t)$ with $a_2 = 0, \ldots, a_n = 0$, and adopting $W_1 = 1$ and $W_i = 0$ for $I = 2, \ldots, n$ in order to approximate the temperature distribution in a half-space whose surface $x = 0$ is heated or cooled, then the system of Eq. (26) is reduced to a single equation:

$$\int_0^{\delta(t)}\left[\tilde{q} + k(\tilde{T})\frac{\partial \tilde{T}}{\partial x}\right]dx = 0. \tag{28}$$

Equation (28) is a counterpart to the classic HBIM method proposed by Goodman [9]. It should be expected that the approximate temperature profile determined using Eq. (28) will be more accurate for temperature-dependent conductivity than the temperature profile determined using the classical HBIM. In the classical HBIM, given by Eq. (8), in the heat balance equation for the analysed area, thermal conductivity is calculated only at the boundary temperature of the area, while in Eq. (28) the variability $k(T)$ is taken into account throughout the entire area. It should be noted that the classical HBIM method is obtained from Eq.(15) by assuming $W_1 = 1$, $W_2 = W_3 =, \ldots, = W_n = 0$.

The proposed method, as given by Eqs. (28) and (27), is referred to as the heat flux integral method (HFIM). The advantage of HFIM over HBIM is its greater accuracy in solving heat conduction problems, especially for bodies with position- or temperature-dependent thermal conductivity. HFIM applied to one-dimensional heat conduction problems is characterised by a high degree of transparency in the derivation of formulas for calcu-

lating transient temperature distributions and requires little more work than HBIM given by Eq. (8), which is formulated for the heat conduction equation.

Section 4 presents the application of the HFIM, HBIM and FVM methods to determine the transient temperature field in a plate and in a straight fin of constant thickness, taking into account the linear dependence of the thermal conductivity on temperature. The fin efficiency was also determined using the three methods mentioned above: HBIM, HFIM and FVM.

4. Examples of application of HFIM and HBIM for determining the temperature distributions in a plate and fin with temperature-dependent thermal conductivity

First, the transient temperature distribution in a plate with temperature-dependent thermal conductivity will be determined using three different methods, HBIM, HIFM and FEM.

4.1. Transient temperature distribution in a plate with temperature-dependent thermal conductivity

The thermal conductivity of the plate $k(T)$ is linearly dependent on temperature, and the density ρ and specific heat c are constant. The initial temperature of the plate is constant and equals T_0. The front surface of the plate with coordinate $x = 0$ for time $t > 0$ is constant and equals $T_s > T_0$, i.e., the change in the temperature of the plate surface is described by the Heaviside step function. The rear surface of the plate is thermally insulated. The transient temperature distribution in the plate is determined using the non-linear heat conduction equation:

$$\frac{\partial\theta}{\partial \mathrm{Fo}} = \frac{\partial}{\partial X}\left[K(\theta)\frac{\partial\theta}{\partial X}\right], \quad 0 < \mathrm{Fo}, \quad 0 \le X \le 1. \tag{29}$$

The dimensionless thermal conductivity is:

$$K(\theta) = 1 + \beta\theta. \tag{30}$$

Equation (29) is subject to the following boundary conditions:

$$\theta|_{X=0} = 1, \tag{31}$$

$$\left.\frac{\partial\theta}{\partial X}\right|_{X=1} = 0, \tag{32}$$

and the initial condition:

$$\theta|_{\mathrm{Fo}=0} = 0. \tag{33}$$

In Eqs. (29)–(33), the following symbols are used: $\theta = \frac{T-T_0}{T_s-T_0}$, $\mathrm{Fo} = \frac{\alpha_0 t}{L^2}$, $X = \frac{x}{L}$, $K = \frac{k}{k_0} = 1 + \beta\theta$, $k_0 = k(T_0)$, $\alpha_0 = \frac{k_0}{c\rho}$, and β is a constant.

The unsteady temperature distribution in the slab was determined using HFIM, HBIM and FVM in conjunction with the method of lines [26].

4.1.1. Determination of the unsteady temperature distribution in the plate using the HFIM method

If the concept of heat penetration depth is used, the plate heating process is divided into two phases (Fig. 1).

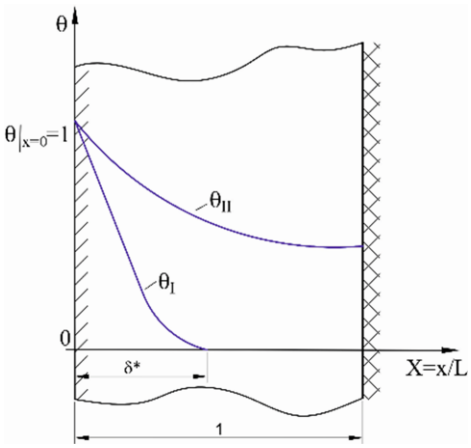

Fig. 1. Temperature distribution in the first and second phases of heat penetration.

The depth of heat penetration in the first phase is less than the thickness of the plate, and from the beginning of the second phase, the temperature of the rear surface of the plate increases (Fig. 1). In the first phase of heat penetration, when the depth of heat penetration $\delta(t)$ is less than or equal to the wall thickness L, the temperature distribution is approximated by a quadratic polynomial with respect to X:

$$\tilde{\theta}_I = aX^2 + bX + c, \qquad 0 \le X \le \delta^*, \tag{34}$$

where $\delta^* = \delta/L$.

The constants a, b and c are determined from the boundary condition (31) and from the conditions of zero temperature and heat flux at the point $X = \delta^*$:

$$\tilde{\theta}_I\big|_{X=\delta^*} = 0, \tag{35}$$

$$\left.\frac{\partial\tilde{\theta}_I}{\partial X}\right|_{X=\delta^*} = 0. \tag{36}$$

After determining the constants in Eq. (34) from boundary conditions (31), (35) and (36), and substituting them back into Eq. (34), the following temperature distribution is obtained:

$$\tilde{\theta}_I = \left(1 - \frac{X}{\delta^*}\right)^2, \qquad 0 \le X \le \delta^*, \tag{37}$$

$$\tilde{\theta}_I = 0, \qquad \delta^* \le X \le 1. \tag{38}$$

The dimensionless heat flux is determined using Eq. (27) written in dimensionless form with $\dot{q}_v = 0$:

$$\tilde{q}^*_I = -\int \frac{\partial\tilde{\theta}_I}{\partial \mathrm{Fo}} dX + C. \tag{39}$$

Considering that:

$$\frac{\partial\tilde{\theta}_I}{\partial \mathrm{Fo}} = 2\left(1 - \frac{X}{\delta^*}\right)\frac{X}{(\delta^*)^2}\frac{d\delta^*}{d\mathrm{Fo}}, \tag{40}$$

and determining a constant C in Eq. (39) from the condition:

$$\tilde{q}^*\big|_{X=\delta^*} = 0, \tag{41}$$

the following is obtained from Eq. (39):

$$\tilde{q}^*{}_I = \left[\left(1-\frac{X}{\delta^*}\right)^2 - \frac{2}{3}\left(1-\frac{X}{\delta^*}\right)^3\right]\frac{d\delta^*}{d\mathrm{Fo}} = \\ = \left[\frac{1}{3} - \left(\frac{X}{\delta^*}\right)^2 + \frac{2}{3}\left(\frac{X}{\delta^*}\right)^3\right]\frac{d\delta^*}{d\mathrm{Fo}}. \tag{42}$$

According to HFIM, the dimensionless heat penetration depth $\delta^* = \delta/L$ is determined from Eq. (28) written in dimensionless form, which in this case is:

$$\int_0^{\delta^*}\left[\tilde{q}^*{}_I + K(\tilde{\theta}_I)\frac{\partial\tilde{\theta}_I}{\partial X}\right]dX = 0. \tag{43}$$

After substituting Eqs. (37), (38), and Eq. (42) into Eq. (43) and taking into account that $K(\tilde{\theta}_I) = 1 + \beta\tilde{\theta}_I$, the following equation is obtained for determination of δ^*:

$$\frac{d\delta^*}{d\mathrm{Fo}} = \frac{3(2+\beta)}{\delta^*}. \tag{44}$$

The solution of Eq. (44) with initial condition:

$$\delta^*|_{\mathrm{Fo}=0} = 0 \tag{45}$$

has the following form:

$$\delta^* = \sqrt{6(2+\beta)\mathrm{Fo}}. \tag{46}$$

The first phase of heat penetration ends when $\delta^* = 1$. The value of the Fourier number Fo_1 at which the first phase of heat penetration ends and the second phase begins is determined from Eq. (46) after substitution $\delta^* = 1$:

$$\mathrm{Fo}_1 = \frac{1}{6(2+\beta)}. \tag{47}$$

Next, the temperature distribution in the plate during the second phase of heat penetration was determined.

During the second phase of heat penetration (Fig. 1), the temperature distribution $\tilde{\theta}_{II}(X, Fo)$ in the plate was approximated by a second-degree polynomial of X:

$$\tilde{\theta}_{II} = gX^2 + fX + e, \qquad 0 \le X \le 1, \qquad \mathrm{Fo}_1 \le \mathrm{Fo}, \tag{48}$$

where the symbols e, f, and g denote coefficients. After determining the coefficients f and e from boundary conditions, given by Eq. (35) and Eq. (36), and substituting them back into Eq. (48), one gets:

$$\tilde{\theta}_{II} = gX^2 - 2gX + 1, \qquad 0 \le X \le 1, \qquad \mathrm{Fo}_1 \le \mathrm{Fo}. \tag{49}$$

The constant g in Eq. (49) was determined using HFIM.

To determine the function $g(\mathrm{Fo})$ in the assumed temperature profile, HFIM is used, which in the second phase of heat penetration has the following form:

$$\int_0^1\left[\tilde{q}^*{}_{II} + K(\tilde{\theta}_{II})\frac{\partial\tilde{\theta}_{II}}{\partial X}\right]dX = 0. \tag{50}$$

The dimensionless heat flux is determined by using Eq. (27) written in dimensionless form with $\dot{q}_v = 0$:

$$\tilde{q}^*{}_{II} = -\int\frac{\partial\tilde{\theta}_{II}}{\partial\mathrm{Fo}}dX + C. \tag{51}$$

Considering that:

$$\frac{\partial\tilde{\theta}_{II}}{\partial\mathrm{Fo}} = (X^2 - 2X)\frac{dg}{d\mathrm{Fo}}, \tag{52}$$

and determining a constant C in Eq. (51) from the condition:

$$\tilde{q}^*\big|_{X=1} = 0 \tag{53}$$

the following is obtained from Eq. (51):

$$\tilde{q}^*{}_{II} = -\left(\frac{1}{3}X^3 - X^2 + \frac{2}{3}\right)\frac{dg}{d\mathrm{Fo}}. \tag{54}$$

Considering the temperature profile $\tilde{\theta}_{II}$ given by Eq. (49), the second term in Eq. (50) can be derived:

$$K(\tilde{\theta}_{II})\frac{\partial\tilde{\theta}_{II}}{\partial X} = 2g[1+\beta(gX^2 - 2gX + 1)](X-1) = \\ = 2g(X-1) + 2g\beta(X-1)(gX^2 - 2gX + 1). \tag{55}$$

Substituting Eq. (54) and Eq. (55) into Eq. (50) and performing integration gives the following differential equation:

$$\frac{5}{g[6\beta g - 12(1+\beta)]}\frac{dg}{d\mathrm{Fo}} = 1. \tag{56}$$

Equation (56) is subject to the following initial condition at the beginning of the second phase of heat penetration:

$$g(\mathrm{Fo})|_{\mathrm{Fo}=\mathrm{Fo}_1} = 1. \tag{57}$$

The solution to Eq. (56) with the initial condition (57) is:

$$ln\frac{(\beta+2)g}{-\beta g + 2\beta + 2} = -\mu^2(Fo - \mathrm{Fo}_1), \qquad \mathrm{Fo} \ge \mathrm{Fo}_1, \tag{58}$$

where

$$\mu^2 = \frac{12(1+\beta)}{5}. \tag{59}$$

Solving the algebraic Eq. (58) for g yields:

$$g(\mathrm{Fo}) = \frac{2(1+\beta)\,exp[-\mu^2(\mathrm{Fo}-\mathrm{Fo}_1)]}{2+\beta+\beta\,exp[-\mu^2(\mathrm{Fo}-\mathrm{Fo}_1)]}, \qquad \mathrm{Fo} \ge \mathrm{Fo}_1. \tag{60}$$

Analysis of Eq. (49) shows that the function $g(\mathrm{Fo})$ has a physical interpretation, since the temperature of the rear surface of the plate is:

$$\theta|_{X=1} = 1 - g, \qquad \mathrm{Fo} \ge \mathrm{Fo}_1. \tag{61}$$

4.1.2. Determination of the transient temperature distribution in the plate using the HBIM method

In HBIM, the heat conduction Eq. (29) is integrated. In the first phase of heat penetration, the depth of heat penetration $\delta^*(\mathrm{Fo})$ is determined from the equation:

$$\int_0^{\delta^*}\frac{\partial\tilde{\theta}_I}{\partial\mathrm{Fo}}dX = \int_0^{\delta^*}\frac{\partial}{\partial X}\left[K(\tilde{\theta}_I)\frac{\partial\tilde{\theta}_I}{\partial X}\right]dX, \qquad 0 \le X \le 1. \tag{62}$$

Using the Leibniz integral rule [22] for differentiation of a definite integral at the left side of Eq.(62) and integrating the right side of Eq. (62) gives:

$$\frac{d}{d\mathrm{Fo}}\int_0^{\delta^*}\tilde{\theta}_I dX = K(\tilde{\theta}_I)\frac{\partial\tilde{\theta}_I}{\partial X}|X=\delta^* - K(\tilde{\theta}_I)\frac{\partial\tilde{\theta}_I}{\partial X}|X=0. \quad (63)$$

Due to condition (36), the first term on the right-hand side of Eq. (63) is equal to zero, and Eq. (63) simplifies to the form:

$$\frac{d}{d\mathrm{Fo}}\int_0^{\delta^*}\tilde{\theta}_I dX = -K(\tilde{\theta}_I)\frac{\partial\tilde{\theta}_I}{\partial X}|X=0. \quad (64)$$

After considering Eqs. (37) and (38) in the heat balance equation (64), one obtains:

$$\frac{d}{d\mathrm{Fo}}\int_0^{\delta^*}\left(1-\frac{X}{\delta^*}\right)^2 dX = -(1+\beta)\left(\frac{-2}{\delta^*}\right). \quad (65)$$

After determining the integral in Eq. (65), a differential equation is obtained, which, after integration with the initial condition (45), gives the following result:

$$\delta^* = \sqrt{12(1+\beta)\mathrm{Fo}}. \quad (66)$$

The first phase of heat penetration ends when the depth of heat penetration δ equals the wall thickness L. The Fourier number Fo_1 at which the first phase of heat penetration ends and the second phase begins is obtained by assuming $\delta^* = 1$ in Eq. (66). Substituting $\delta^* = 1$ into Eq. (66) gives:

$$\mathrm{Fo}_1 = \frac{1}{12(1+\beta)}. \quad (67)$$

Next, the temperature distribution in the second phase of heat penetration was determined. The temperature distribution in the second phase is given by the function (49). The unknown parameter $g(t)$ was determined by HBIM using the following equation:

$$\int_0^1\left\{\frac{\partial\tilde{\theta}_{II}}{\partial\mathrm{Fo}} - \frac{\partial}{\partial X}\left[K(\tilde{\theta}_{II})\frac{\partial\tilde{\theta}_{II}}{\partial X}\right]\right\}dX = 0, \quad 0 \le X \le 1. \quad (68)$$

The following heat balance equation is obtained from the integral (68), taking into account Eq. (32):

$$\frac{d}{d\mathrm{Fo}}\int_0^1\tilde{\theta}_{II}dX = -K(\tilde{\theta}_{II})\frac{\partial\tilde{\theta}_{II}}{\partial X}|x=0, \quad 0 \le X \le 1. \quad (69)$$

After substituting Eq. (49) into Eq. (69) and performing the calculations, the following differential equation is obtained for $g(\mathrm{Fo})$:

$$\frac{dg}{dFo} = -3(1+\beta). \quad (70)$$

Integrating Eq. (70) with initial condition (57) gives:

$$g(\mathrm{Fo}) = exp[-\mu_1^2(\mathrm{Fo}-\mathrm{Fo}_1)], \quad \mathrm{Fo}_1 \le \mathrm{Fo}, \quad (71)$$

where:

$$\mu_1^2 = 3(1+\beta), \quad \mathrm{Fo}_1 = \frac{1}{12(1+\beta)}. \quad (72)$$

To assess the accuracy of temperature distributions determined using the HFIM and HBIM methods, the transient temperature distribution in the plate was calculated using the method of lines, where the partial heat conduction equation is replaced by a system of first-order ordinary differential equations.

4.1.3. Determination of the unsteady temperature distribution in the plate using FVM in conjunction with the method of lines

The method of lines [26] involves replacing a partial differential equation with a system of ordinary differential equations, which can then be solved using one of the many numerical methods available in the literature. The finite volume method (FVM) [15,23] was used to replace the transient heat conduction equation (29) with a system of ordinary differential equations. The division of the wall into (n–1) finite volumes is shown in Fig. 2. The symbol n denotes the number of nodes at which the wall temperatures are determined.

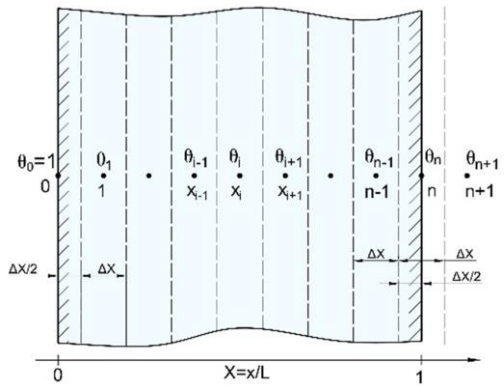

Fig. 2. Division of the wall into n finite volumes.

The coordinates of the nodes (Fig. 2) are defined as follows:

$$X_i = i\Delta X, \qquad i = 0, \ldots, n, \quad (73)$$

where the thickness of a single finite volume is:

$$\Delta X = \frac{1}{n-1}. \quad (74)$$

Integrating Eq. (29) over the thickness of one control volume within the range from ($X_i - \Delta X/2$) to ($X_i + \Delta X/2$) gives:

$$\Delta X\frac{d\theta_i}{d\mathrm{Fo}} = \frac{K(\theta_{i+1})+K(\theta_i)}{2}\frac{\theta_{i+1}-\theta_i}{\Delta X} + \frac{K(\theta_{i-1})+K(\theta_i)}{2}\frac{\theta_{i-1}-\theta_i}{\Delta X}, \quad (75)$$
$$i = 2, \ldots, n.$$

Considering that:

$$\frac{K(\theta_{i+1})+K(\theta_i)}{2} = 1+\beta\frac{\theta_i+\theta_{i+1}}{2}, \quad (76)$$

and

$$\frac{K(\theta_{i-1})+K(\theta_i)}{2} = 1+\beta\frac{\theta_i+\theta_{i-1}}{2}. \quad (77)$$

Equation (75) can be written as:

$$\frac{d\theta_i}{d\mathrm{Fo}} = \left(1+\beta\frac{\theta_i+\theta_{i+1}}{2}\right)\frac{\theta_{i+1}-\theta_i}{(\Delta X)^2} + \left(1+\beta\frac{\theta_i+\theta_{i-1}}{2}\right)\frac{\theta_{i-1}-\theta_i}{(\Delta X)^2}, \quad (78)$$
$$i = 2, \ldots, n.$$

The boundary condition (31) implies that at node $i = 0$, the temperature is known:

$$\theta_0 = 1. \tag{79}$$

For nodes $i = 2, \ldots, n-1$, the system of differential equations is defined by Eq. (78). The differential equation for node $i = n$ contains the temperature θ_{n+1} at the apparent node $i = n + 1$. It can be eliminated using the boundary condition (32). Approximating the derivative in Eq. (32) by the central difference quotient gives:

$$\frac{\theta_{n+1}-\theta_{n-1}}{2\Delta X} = 0. \tag{80}$$

Equation (80) yields:

$$\theta_{n+1} = \theta_{n-1}. \tag{81}$$

Equation (78) has the following form after taking into account Eq. (81) for $i = n$:

$$\frac{d\theta_n}{d\mathrm{Fo}} = 2\left(1 + \beta\frac{\theta_{n-1}+\theta_n}{2}\right)\frac{\theta_{n-1}-\theta_n}{(\Delta X)^2}. \tag{82}$$

The system of differential equations consisting of Eqs. (78) for $i = 1, \ldots, n-1$ and Eq. (82) with consideration of Eq. (79) was solved using the fourth-order Runge-Kutta method with the following initial condition:

$$\theta_i|_{t=0} = 0, \qquad i = 0, \ldots, n. \tag{83}$$

The calculations were performed using $n = 51$ and a dimensionless time step $\Delta\mathrm{Fo} = 0.00005$. The transient temperature distribution in the plate was determined in the dimensionless time interval $0 \leq \mathrm{Fo} \leq 1.0$.

Next, in Subsection 4.2, the temperature distribution and efficiency of a straight fin with a constant thickness and temperature-dependent thermal conductivity will be determined.

4.2. Temperature distribution and efficiency of a straight fin with a constant thickness and temperature-dependent thermal conductivity

The steady-state temperature distribution in the fin and its efficiency were determined using HFIM, HBIM and FVM, which allowed the accuracy of the solutions obtained using HFIM and HBIM to be assessed. The fin shown in Fig. 3, with a thermal conductivity that is linearly dependent on temperature, was analysed.

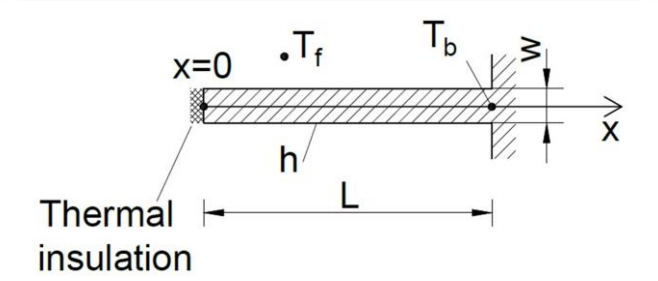

Fig. 3. Straight fin of constant thickness with insulated tip.

The symbols in Fig. 3 denote: h – HTC, L – fin height, T_b – fin base temperature, T_f – fluid temperature, w – fin thickness, x – Cartesian coordinate.

The governing heat conduction equation in a fin is:

$$\frac{d}{dx}\left[k(T)\frac{dT}{dx}\right] - \frac{2h}{w}(T - T_f) = 0. \tag{84}$$

The thermal conductivity of the fin material $k(T)$ is a linear function of the fin temperature and is given by the function:

$$k(T) = k(T_f)\left[1 + \beta_k(T - T_f)\right], \tag{85}$$

where the symbol β_k denotes a constant.

Equation (84) is subject to the following boundary conditions:

$$T|_{x=L} = T_b, \tag{86}$$

$$\left.\frac{\partial T}{\partial x}\right|_{x=0} = 0. \tag{87}$$

Introducing dimensionless variables:

$$\theta = \frac{T-T_f}{T_b-T_f}, \qquad X = \frac{x}{L}, \qquad N^2 = \frac{2hL^2}{k(T_f)w}$$

$$\varepsilon = \frac{k(T_b)-k(T_f)}{k(T_f)} = \beta_k(T_b - T_f), \tag{88}$$

Eqs. (84), (86) and (87) can be written in the following form:

$$\frac{d}{dX}\left[(1 + \varepsilon\theta)\frac{d\theta}{dX}\right] - N^2\theta = 0, \tag{89}$$

$$\theta|_{X=1} = 1, \tag{90}$$

$$\left.\frac{d\theta}{dX}\right|_{X=0} = 0. \tag{91}$$

4.2.1. Determination of temperature distribution in a fin using the HBIM method

The temperature distribution is approximated by the function [27]:

$$\tilde{\theta} = \frac{\cosh NX}{\cosh N} + C\left(\frac{\cosh 2NX}{\cosh\ 2N} - \frac{\cosh NX}{\cosh N}\right), \tag{92}$$

where C is a constant.

The constant C was determined using HFIM, i.e., from the following equation:

$$\int_0^1 \left[\tilde{q} + \left(1 + \varepsilon\tilde{\theta}\right)\frac{d\tilde{\theta}}{dX}\right] dX = 0. \tag{93}$$

To determine the heat flux, Eq. (89) was written in the form:

$$\frac{d\tilde{q}}{dX} + N^2\tilde{\theta} = 0. \tag{94}$$

Equation (94) is subject to the following boundary condition at the fin tip:

$$\tilde{q}|_{X=0} = 0. \tag{95}$$

After substituting the temperature distribution given by Eq. (92) into Eq. (94) and integrating this equation, considering

the boundary condition given by Eq.(95), an expression for the heat flux is obtained:

$$\tilde{q} = -N\left[\frac{sinh\,NX}{cosh\,N} + C\left(\frac{sinh2NX}{2cosh2N} - \frac{sinh\,NX}{cosh\,N}\right)\right]. \quad (96)$$

The second term under the integral in Eq. (93) is:

$$\left(1+\varepsilon\tilde{\theta}\right)\frac{d\tilde{\theta}}{dX} = \left(1+\varepsilon\frac{cosh\,NX}{cosh\,N} + C\varepsilon\frac{cosh\,2NX}{cosh\,2N} - C\varepsilon\frac{cosh\,NX}{cosh\,N}\right)\times$$
$$\times\left(\frac{N\,sinh\,NX}{cosh\,N} + C\frac{2Nsinh2NX}{cosh\,2N} - C\frac{N\,sinh\,NX}{cosh\,N}\right). \quad (97)$$

After substituting Eq. (96) and Eq. (97) into Eq. (93), the following second-degree algebraic equation is obtained to determine the constant C

$$\alpha_c C^2 + \beta_c C + \gamma_c = 0. \quad (98)$$

The constants α_c, β_c, and γ_c are given by the following expressions:

$$\alpha_c = \frac{\varepsilon\,sinh^2\,2N}{2\,cosh^2\,2N} - \frac{\varepsilon(cosh\,N-1)}{cosh\,N\,cosh\,2N} - \frac{2\varepsilon\,sinh^2\,N}{cosh\,2N} + \frac{\varepsilon\,sinh^2\,N}{2\,cosh^2\,N}, \quad (99)$$

$$\beta_c = \frac{3\,sinh^2\,N}{2\,cosh\,2N} + \frac{\varepsilon(cosh\,N-1)}{cosh\,N\,cosh\,2N} + \frac{2\varepsilon\,sinh^2\,N}{cosh\,2N} - \frac{\varepsilon\,sinh^2\,N}{cosh^2\,N}, \quad (100)$$

$$\gamma_c = \frac{\varepsilon\,sinh^2\,N}{2\,cosh^2\,N}. \quad (101)$$

A solution to Eq. (98) that makes physical sense is:

$$C = \frac{-\beta_c + \sqrt{\beta_c^2 - 4\alpha_c\gamma_c}}{2\alpha_c}. \quad (102)$$

The fin efficiency η, defined as the ratio of the heat flow rate dissipated by the actual fin to the maximum heat flow rate dissipated by an isothermal fin at temperature T_b, is calculated using the following formula:

$$\eta = \int_0^1 \tilde{\theta}(X)\,dX = \frac{tanh\,N}{N}\left(1 - C\frac{tanh^2\,N}{1+tanh^2\,N}\right). \quad (103)$$

Next, the temperature distribution in the fin and its efficiency will be determined using HBIM.

4.2.2. Determination of temperature distribution in a fin using the HBIM method

In the case of HBIM, the constant C in Eq. (103) is determined using the following equation:

$$\int_0^1 \left\{\frac{d}{dX}\left[\left(1+\varepsilon\tilde{\theta}\right)\frac{d\tilde{\theta}}{dX}\right] - N^2\tilde{\theta}\right\}dX = 0. \quad (104)$$

After substituting the function $\tilde{\theta}$, given by Eq. (92), approximating the temperature distribution in the fin, into Eq. (104), and performing the operations, the following formula for calculating the constant C is obtained:

$$C = \frac{\varepsilon\,tanh\,N}{\varepsilon\,tanh\,N - 2(1+\varepsilon)\,tanh\,2N + \frac{1}{2}tanh\,2N}. \quad (105)$$

4.2.3. Determination of temperature distribution in a fin using the FVM method

The FVM was used to determine the temperature distribution in the fin analysed. Examples of application of FVM for calculating the temperature field in straight and circular fins with constant thermal conductivity are presented in [28]. The division of the analysed fin into finite volumes is illustrated in Fig. 4.

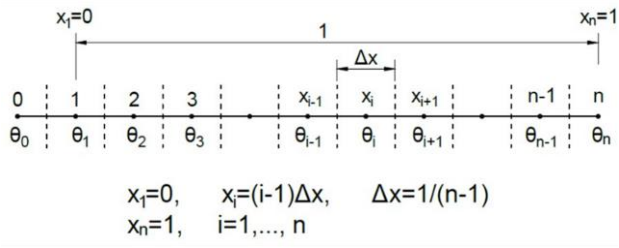

Fig. 4. Division of the fin into finite volumes.

The coordinates of the nodes are defined as follows:

$$X_i = (i-1)\Delta X, \quad \Delta X = 1/(n-1), \quad i = 1,\ldots,n. \quad (106)$$

According to the FVM method, Eq. (89) is integrated in the range from ($X_i - \Delta X/2$) to ($X_i + \Delta X/2$):

$$\int_{X_i-\Delta X/2}^{X_i+\Delta X/2}\left\{\frac{d}{dX}\left[\left(1+\varepsilon\theta\right)\frac{d\theta}{dX}\right] - N^2\theta\right\}dX = 0,$$
$$i = 1,\ldots,n-1. \quad (107)$$

Integrating Eq. (107) gives:

$$\left[\left(1+\varepsilon\theta\right)\frac{d\theta}{dX}\right]\Big|_{X_i+\Delta X/2} - \left[\left(1+\varepsilon\theta\right)\frac{d\theta}{dX}\right]\Big|_{X_i-\Delta X/2} - N^2\theta_i\Delta X = 0,$$
$$i = 1,\ldots,n-1. \quad (108)$$

Approximating the derivatives in Eq. (108) by forward difference quotients, one obtains after transformations:

$$\theta_i = \frac{1}{2+\varepsilon\frac{\theta_{i-1}+2\theta_i+\theta_{i+1}}{2}+N^2(\Delta X)}\cdot$$
$$\left[\left(1+\varepsilon\frac{\theta_{i-1}+\theta_i}{2}\right)\theta_{i-1} + \left(1+\varepsilon\frac{\theta_i+\theta_{i+1}}{2}\right)\theta_{i+1}\right], \quad (109)$$
$$i = 1,\ldots,n-1.$$

The equation for the first node is derived taking into account the boundary condition (91). Approximating the derivative in Eq. (91) with the central difference quotient gives:

$$\frac{\theta_2-\theta_0}{2\Delta X} = 0. \quad (110)$$

It follows from Eq. (110) that:

$$\theta_0 = \theta_2. \quad (111)$$

Considering Eq. (111) in Eq. (109) for i=1 gives:

$$\theta_1 = \frac{2\left(1+\varepsilon\frac{\theta_1+\theta_2}{2}\right)\theta_2}{2+\varepsilon(\theta_1+\theta_2)+N^2(\Delta X)^2}. \quad (112)$$

It follows from Eq. (90) that:

$$\theta_n = 1. \tag{113}$$

The system of equations consisting of Eq. (112), Eq. (109) for i = 2, …, n−1 and Eq. (113) was solved using the Gauss-Seidel iterative method [15,29]. The temperature in the fin was determined at n = 51 nodes, i.e., the fin was divided into (n−1) = 50 finite volumes. As a first approximation, it was assumed that the temperature of the fin at all nodes is equal to the temperature of the fin base, i.e., $\theta_i^{(0)} = 1.0$, i = 1, …, n. Then, after determining the temperature distribution, the efficiency η of the fin is determined

$$\eta = \int_0^1 \theta dX = \frac{\theta_1 \Delta X}{2} + \sum_{i=2}^{n-1} \theta_i \Delta X + \frac{\theta_n \Delta X}{2}. \tag{114}$$

The rectangle method was used to calculate the integral in Eq. (114).

In Section 5, HFIM and HBIM are compared using the examples of determining the transient temperature field in a plate and the steady-state temperature field in a straight fin of constant thickness made of a material with a temperature-dependent thermal conductivity. The temperature distributions and fin efficiency determined by HFIM and HBIM were also compared with numerical solutions.

5. Comparison of temperature distributions in the plate and fin obtained by HFIM, HBIM and FVM

5.1. Comparison of the unsteady temperature distribution in the plate obtained by HFIM, HBIM and numerical method of lines

The transient temperature distributions in the plate determined using HFIM and HBIM were compared with the numerical solution. The temperature distributions obtained from HFIM and HBIM during the first (Figs. 5−7) and second phase (Figs. 8, 9) of heat penetration were analysed. Temperature changes across the plate thickness are shown in Figs. 5a−7b for the first phase of heat penetration at Fourier number values of Fo = 0.004, 0.03, 0.05, and in Figs. 8, 9 for the second phase at Fo = 0.2 and 0.8.

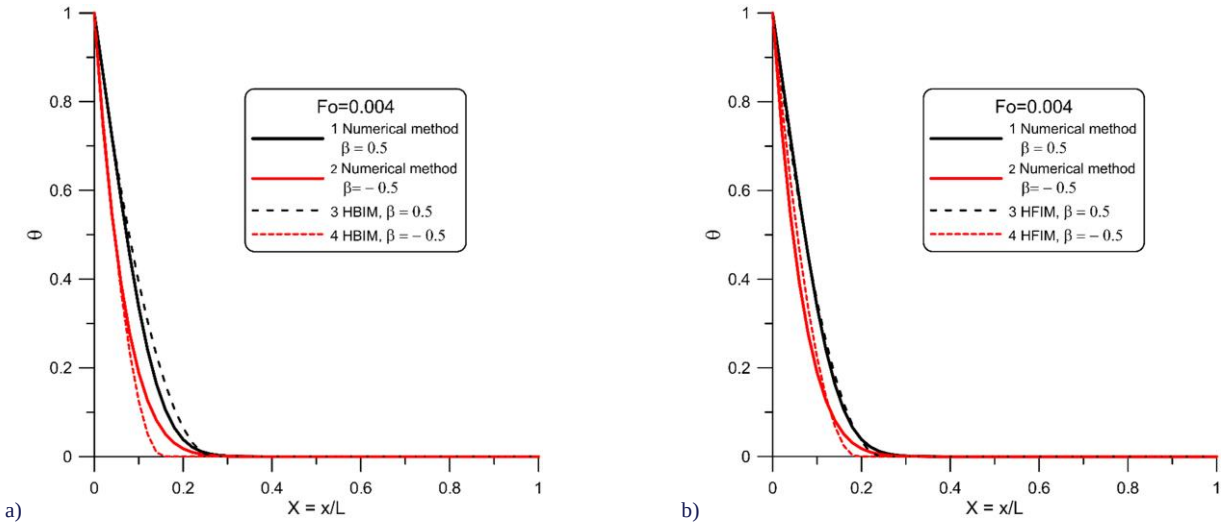

Fig. 5. Temperature distribution in the plate during the first phase of heat penetration for Fo = 0.004.

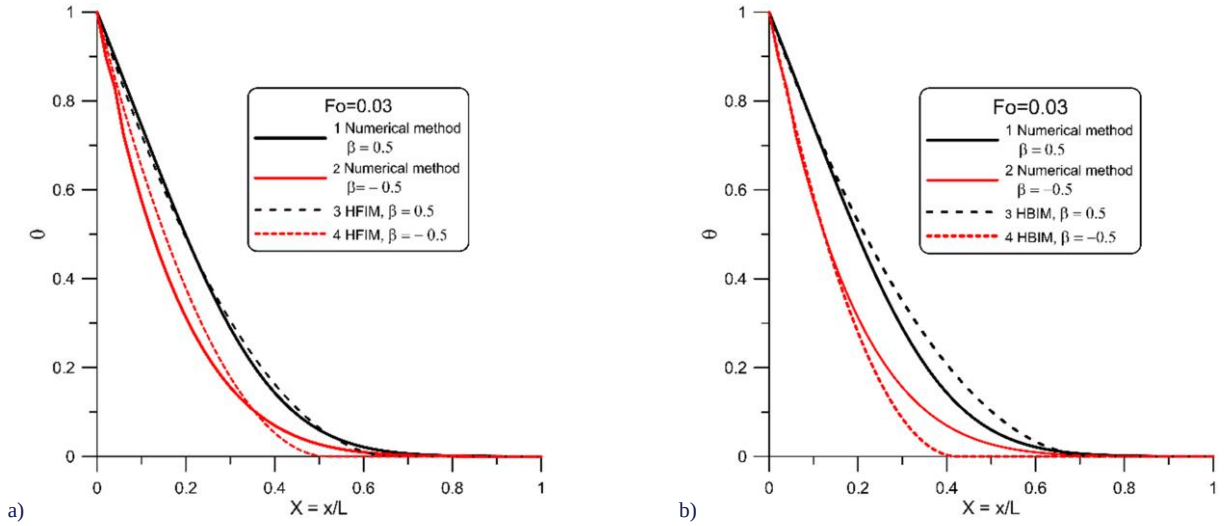

Fig. 6. Temperature distribution in the plate during the first phase of heat penetration for Fo = 0.03.

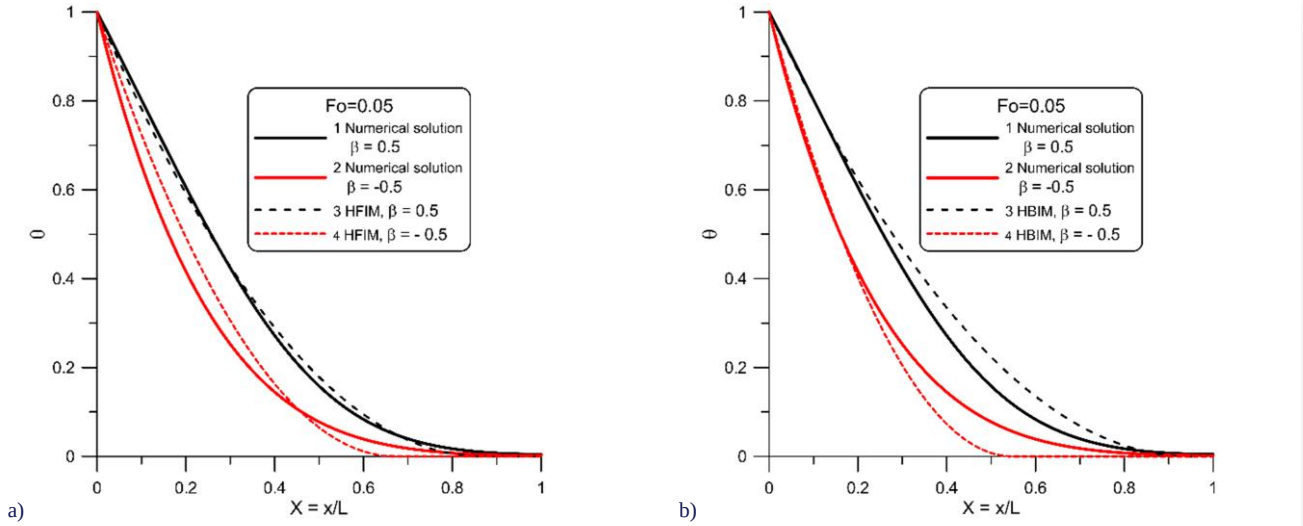

Fig. 7. Temperature distribution in the plate during the first phase of heat penetration for Fo = 0.05.

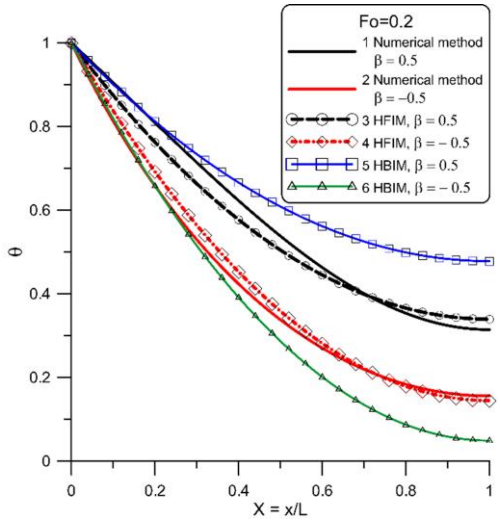

Fig. 8. Temperature distribution in the plate during the second phase of heat penetration for Fo = 0.2.

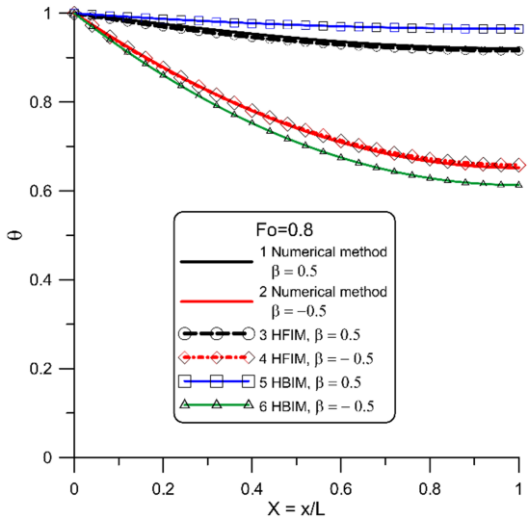

Fig. 9. Temperature distribution in the plate during the second phase of heat penetration for Fo = 0.8.

An analysis of results presented in Figs. 5–9 shows that HFIM provides more accurate results compared to HBIM. Both HFIM and HBIM are more accurate in determining the temperature distribution for $\beta = 0.5$ when the thermal conductivity increases with increasing temperature, compared to the case $\beta = -0.5$ when the thermal conductivity decreases with increasing temperature. The difference between the plate temperature calculated numerically $\theta_{i,num}$ and analytically $\theta_{i,app}$ using the HFIM or HBIM is given by:

$$e_{\theta,i} = \theta_{i,num} - \theta_{i,app}\,, \qquad i = 1,\ldots,n, \tag{115}$$

where the symbol n denotes the number of nodes in the thickness of the plate (Fig. 2) when determining the transient temperature in the plate using the finite volume method (FVM).

An inspection of the results presented in Figs. 10a–10e shows that HFIM proposed in the paper gives more accurate results than HBIM. The mean-square temperature difference $\bar{e}_\theta$ between the temperature values $\theta_{i,app}$ calculated by the approximate analytical method, HFIM or HBIM, and the numerical method $\theta_{i,num}$ was obtained using the formula:

$$\bar{e}_\theta = \sqrt{\frac{1}{n}\sum_{i=1}^{n} e_{\theta,i}^2}, \tag{116}$$

where (n+1) denotes the number of nodes in the thickness of the plate (Fig. 2).

In Table 1, the mean square errors $\bar{e}_\theta$ and the maximum errors $\varepsilon_{\theta,max}$ among all n errors calculated using Eqs. (116) and (115) are compared for HFIM and HBIM.

It can be seen from an inspection of Table 1 that both the mean square errors $\bar{e}_\theta$ and maximum errors $\varepsilon_{\theta,max}$ are significantly smaller for the plate temperature determined using HFIM than for those determined using HBIM. In the following example, the temperature distribution and efficiency of a straight fin with a constant thickness and a temperature-dependent thermal conductivity were determined using HFIM, HBIM and the method of lines.

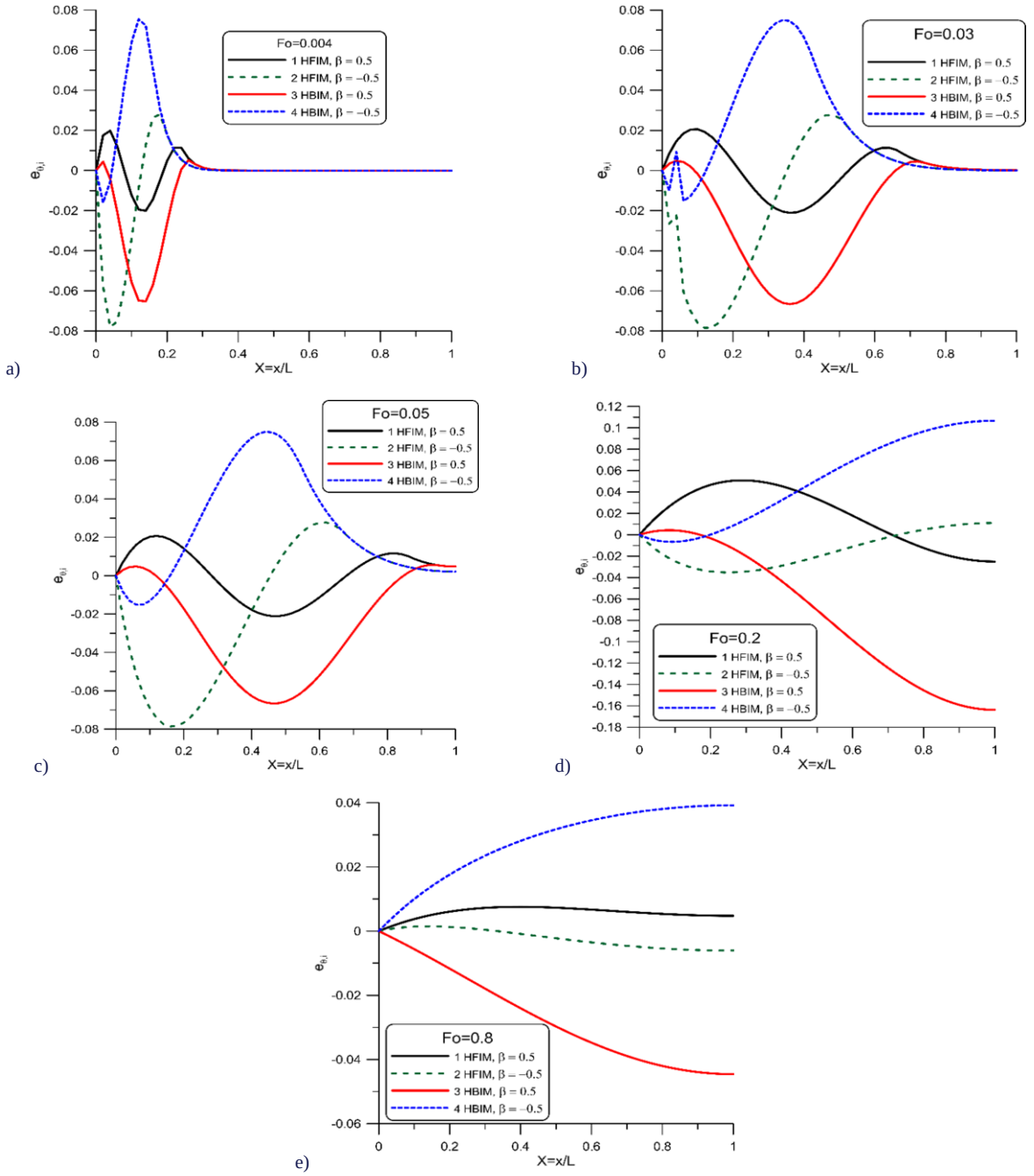

Fig. 10. The difference between the plate temperature calculated numerically $\theta_{i,num}$ and analytically using HFIM or HBIM; a) Fo = 0.004, b) Fo = 0.03, c) Fo = 0.05, d) Fo = 0.2, e) Fo = 0.8.

Table 1. The mean-square temperature difference $\bar{e}_\theta$ between the temperature values $\theta_{i,num}$ calculated numerically using the method of lines and temperatures $\theta_{i,app}$ obtained by approximate analytical methods, HFIM or HBIM.

Fo	Method	$\bar{e}_\theta$		$\lvert e_{\theta,max} \rvert$	
		$\beta = 0.5$	$\beta = -0.5$	$\beta = 0.5$	$\beta = -0.5$
0.004	HFIM	0.0068	0.0207	0.2005	0.0780
	HBIM	0.0196	0.0205	0.0652	0.0754
0.03	HIFM	0.0113	0.0336	0.0206	0.0278
	HBIM	0.0327	0.0333	0.0641	0.0750
0.05	HIFM	0.0129	0.0387	0.0207	0.0786
	HBIM	0.0372	0.0372	0.0664	0.0750
0.2	HIFM	0.0316	0.0212	0.0508	0.0353
	HBIM	0.0966	0.0648	0.1638	0.1067
0.8	HIFM	0.0060	0.0036	0.0076	0.0061
	HBIM	0.0306	0.0300	0.0446	0.0392

5.2. Comparison of the temperature distribution in the fin and the fin efficiency obtained by HFIM, HBIM and FVM

Figure 11a shows a comparison of the temperature distribution obtained using the analytical approximate HFIM presented in the article and using the numerical method FVM. Both methods yield nearly identical results, which demonstrates the high accuracy of HFIM. Inspection of the results presented in Fig. 11b shows that the accuracy of the classical HBIM method is significantly lower than that of the proposed HFIM method, as the differences in fin temperature calculated using FVM and HBIM are greater, especially for $\varepsilon = -0.6$ and $\varepsilon = 0.6$. The reason for the low accuracy of the HBIM method is that the thermal conductivity $K(\theta)$ in the heat balance equation is calculated only at the temperature θ_n of the fin base, i.e. a constant thermal conductivity $K(\theta_n)$ appears in HBIM.

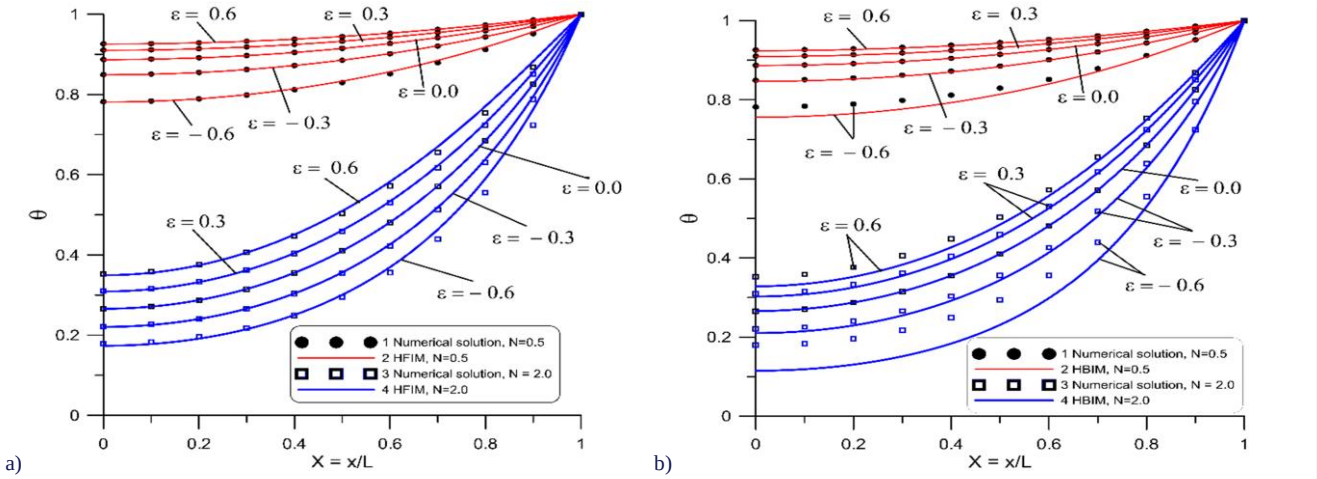

Fig. 11. Comparison of temperature distributions in the fin determined using approximate analytical methods HFIM and HBIM with the temperature distribution determined using the numerical method FVM: a) comparison of temperature distributions determined using HFIM and FVM, b) comparison of temperature distributions determined using HBIM and FVM.

The comparison of the fin efficiency η determined using HFIM and HBIM, with the efficiency determined numerically using FVM as a function of the coefficient ε for different values of the N parameter is presented in Fig. 12.

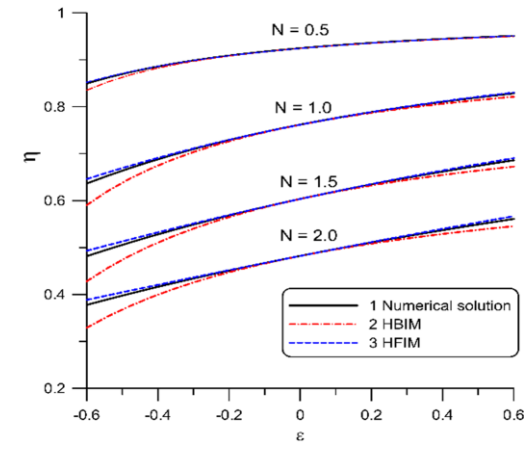

Fig.12. Comparison of the efficiency of the fin determined using HFIM and HBIM with the efficiency determined numerically using FVM as a function of the coefficient ε for different values of parameter N.

The comparison analysis presented in Fig. 12 shows that the efficiency values determined using HFIM are significantly more accurate than those obtained using the HBIM method. The differences between the values η obtained using HBIM and FEM are significant, especially for larger values of the coefficient ε.

To show the differences in fin efficiency η_{anal} determined using HFIM or HBIM and fin efficiency η_{num} determined using FVM, the relative difference e_η was calculated:

$$e_\eta = \frac{\eta_{anal} - \eta_{num}}{\eta_{num}} \cdot 100\%, \qquad (117)$$

where η_{anal} is the fin efficiency determined using the approximate analytical method HFIM or HBIM, and η_{num} denotes the fin efficiency determined numerically using the FVM.

The relative differences e_η for HFIM and HBIM are presented in Figs. 13 and 14, respectively. Figs. 13 and 14 confirm the higher accuracy of HFIM compared to HBIM.

The maximum difference value $|e_\eta|$ for HFIM is approximately 2.9% (Fig. 13), while for HBIM, it is approximately 13% (Fig. 14).

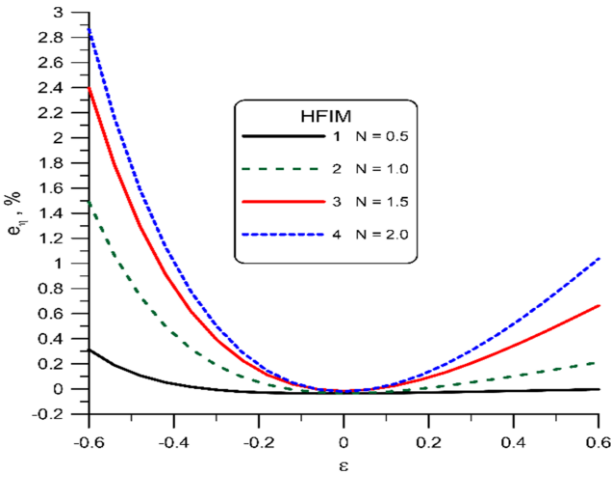

Fig. 13. The relative difference between η_{HFIM} and η_{num} calculated using Eq. (129).

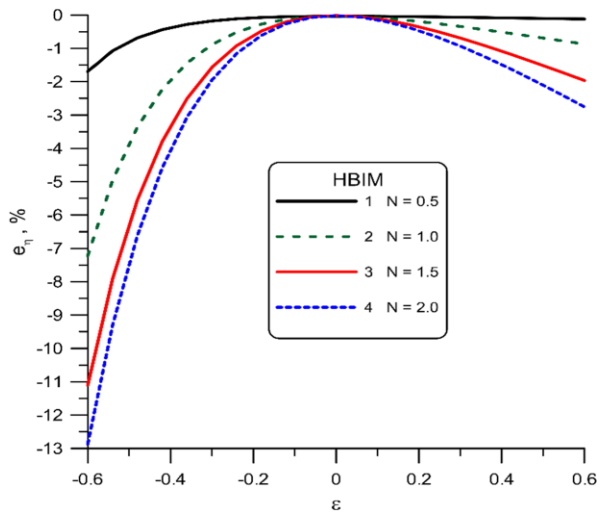

Fig. 14. The relative difference between η_{HBIM} and η_{num} calculated using Eq. (117).

6. Conclusions

This paper presents a new formulation of the method of weighted residuals for Fourier's law of heat conduction. In the case of one-dimensional heat conduction, when the weighting factor equals unity and the concept of a heat penetration depth is applied, the method simplifies to the heat flux integral method (HFIM) proposed. The paper also presents a comparison of the heat balance integral method (HBIM), developed by T.R. Goodman, with HFIM. In HBIM, the transient heat conduction equation is integrated with respect to the spatial coordinate, whereas in HFIM, Fourier's law is integrated over the spatial coordinate. The advantage of HFIM over HBIM is the greater accuracy of determining the temperature distribution, especially in bodies whose thermal conductivity depends on temperature or position. The greater accuracy of the proposed method is illustrated by the determination of the transient temperature distribution in a plate and the steady-state temperature distribution in the fin, both of which involve temperature-dependent thermal conductivity. The temperature distribution in the plate and fin, as well as the fin efficiency, were also determined using the FVM to assess the accuracy of the approximate analytical methods employed in the paper. The advantage of the proposed HFIM is the simplicity of the calculation formulas and the ability to determine the temperature distribution and, if necessary, thermal stresses for arbitrarily small times, i.e., at the beginning of the heating or cooling process of a body. Due to the short calculation time required for computer calculations, the HFIM method can be used to calculate the transient temperature field in thermal stress monitoring systems for pressure components of boilers and turbines.

7. Future work

The proposed weighted residual method for Fourier's law will be applied to approximate the transient temperature and thermal stress distribution in the pressure components of power engineering machinery and equipment. In addition, the application of the proposed method for the approximate determination of two-dimensional steady-state and transient temperature fields in flat, cylindrical and spherical components will be presented.

References

[1] Finlayson, B.A. (2013). *The method of weighted residuals and variational principles* (pp. 397–412). Society for Industrial and Applied Mathematics, 73. doi: 10.1137/1.9781611973242.bm

[2] Taler, J. (1980). *The method of weighted residuals and its application to the calculation of temperature fields in boiler components*, Monograph (14). Cracow University of Technology Press.

[3] Hatami, M. (Ed.). (2017). *Weighted residual methods* (1st ed.). Academic Press. doi: 10.1016/B978-0-12-813218-0.00002-9

[4] Chakraverty, S., Mahato, N.R., Karunakar, P., & Rao, T.D. (2019). *Advanced numerical and semi-analytical methods for differential equations*. John Wiley & Sons. doi: 10.1002/9781119423461

[5] Ganji, D.D., Sabzehmeidani, Y., & Sedighiamiri, A. (2018). *Nonlinear systems in heat transfer: Mathematical modelling and analytical methods* (1st ed.). Elsevier. doi: 10.1016/C2016-0-00401-1

[6] Thomée, V. (2006). *Galerkin finite element methods for parabolic problems* (2nd ed.). Springer. doi: 10.1007/3-540-33122-0

[7] Crank, J. (1980). *The mathematics of diffusion* (2nd ed.). Oxford University Press.

[8] Gibson, W.C. (2021). *The method of moments in electromagnetics* (3rd ed.). Chapman and Hall/CRC. doi: 10.1201/9780429355509

[9] Goodman, T.R. (1964). Application of integral methods to transient nonlinear heat transfer. *Advances in Heat Transfer*, 1, 51−122. doi: 10.1016/S0065-2717(08)70097-2

[10] Pohlhausen, K. (1921). Zur näherungsweisen Integration der Differentialgleichung der laminaren Grenzschicht. *Zeitschrift für Angewandte Mathematik und Mechanik*, 1, 252–268. doi: 10.1002/zamm.19210010401

[11] von Kármán, T. (1921). Über laminare und turbulente Reibung. *Zeitschrift für Angewandte Mathematik und Mechanik*, 1, 233−252. doi: 10.1002/zamm.19210010401

[12] Taler, D., Dzierwa, P., & Taler, J. (2020). New method for determining the optimum fluid temperature when heating pressure thick-walled components with openings. *Energy*, 200, 117527. doi: 10.1016/j.energy.2020.117527

[13] Taler, J., & Taler, D. (2024). Analysis of the possibility of reducing the heating time of thick-walled cylindrical components with holes. *Energy*, 303, 131982. doi: 10.1016/j.energy.2024.131982

[14] Taler, J. (1990). Messung der Wärmebelastung der gasdicht verschweißten Verdampfer-Rohrwände in Dampferzeugern. *VGB Kraftwerkstechnik*, 70, 644–650.

[15] Taler, J., & Duda, P. (2006). *Solving direct and inverse heat conduction problems* (1st ed.). Springer. doi: 10.1007/978-3-540-33471-2

[16] Yener, Y., & Kakaç, S. (2008). *Heat conduction* (4th ed.). Taylor & Francis. doi: 10.1201/9780203752166

[17] Volkov, V.N., & Li-Orlov, V.K. (1970). A refinement of the integral method in solving the heat conduction equation. *Heat Transfer: Soviet Research*, 2, 41–47.

[18] Sitison, J.W., & Edwards, D.A. (2020). The heat balance integral method for cylindrical extruders. *Journal of Engineering Mathematics*, 122, 1–16. doi: 10.1007/s10665-020-10041-y

[19] Kumar, A., & Rajeev. (2021). Heat balance integral method for a time-fractional Stefan problem with Robin boundary condition and temperature-dependent thermal conductivity. *Computational*

Thermal Sciences, 13(6), 71–84. doi: 10.1615/ComputThermalScien.2021038569
[20] Chaurasiya, V., Upadhyay, S., Rai, K.N., & Singh, J. (2022). A new look at the heat balance integral method for a two-dimensional Stefan problem with convection. *Numerical Heat Transfer, Part A: Applications*, 82, 1–14. doi: 10.1080/10407782.2022.2079829
[21] Greenberg, M.D. (1998). *Advanced engineering mathematics* (2nd ed.). Prentice Hall.
[22] Riley, K.F., Hobson, M.P., & Bence, S.J. (2000). *Mathematical methods for physics and engineering* (3rd ed., pp. 124–129). Cambridge University Press. doi: 10.2277/0521861535
[23] Taler, D. (2019). *Numerical modelling and experimental testing of heat exchangers* (1st ed.). Springer Nature. doi: 10.1007/978-3-319-91128-1
[24] Siemens Digital Industries Software. (2025). *Simcenter STAR-CCM+ CFD software*. Munich, Germany.
[25] Ansys, Inc. (2025). *Ansys Fluent: Fluid simulation software.*
[26] Schiesser, W.E. (1991). *The numerical method of lines: Integration of partial differential equations*. Academic Press.
[27] Muzzio, A. (1976). Approximate solution for convective fins with variable thermal conductivity. *Journal of Heat Transfer*, 98, 680–682.
[28] Taler, D. (2014). Fins of straight and circular geometry. In *Encyclopedia of thermal stresses* (pp. 1670–1683). Springer. doi: 10.1007/978-94-007-2739-7
[29] Chapra, S.C., & Canale, R.P. (2010). *Numerical methods for engineers* (6th ed.). McGraw-Hill.

Appendix. Methods for determining one-dimensional steady-state temperature distributions in solids

The purpose of this appendix is to show two different methods of determining temperature distributions in solids. In the first method, the temperature distribution is determined from the energy conservation equation, accounting for Fourier's law. In the second method, the temperature distribution is determined from Fourier's law, and the heat flux is obtained from the energy conservation equation.

In analogy to the second method of determining the temperature distribution, an MWR for Fourier's law has been formulated. The advantage of this approach is that it provides greater accuracy in approximating the temperature distribution than the classical MWR, while requiring a similar amount of work.

Two methods for determining steady-state temperature distributions are presented and illustrated by examples of a cylindrical wall (Fig. A.1) and a spherical wall (Fig. A.2).

In analogy with these methods for determining temperature distributions, two MWRs are formulated: the first based on the law of energy conservation and the second on Fourier's law.

The steady-state temperature distribution in a solid is defined by the equation of energy conservation:

$$\nabla \cdot \dot{\mathbf{q}} = \dot{q}_v. \tag{A.1}$$

The symbol $\dot{q}_v$ denotes the volumetric heat source density in W/m^3. The heat flux $\dot{\boldsymbol{q}}$ is defined by Fourier's law:

$$\dot{\mathbf{q}} = -k\nabla T, \tag{A.2}$$

where the symbol k denotes the thermal conductivity in W/(m·K).

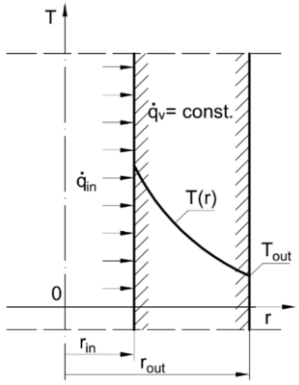

Fig. A.1. Long hollow cylinder subject to heat flux $\dot{q}_{in}$ at the inner surface and temperature T_{out} at the outer surface.

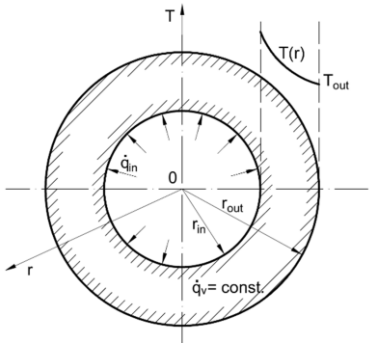

Fig. A.2. Hollow sphere with prescribed heat flux at the inner surface and temperature T_{out} at the outer surface.

To determine the temperature distribution, it is necessary to specify appropriate boundary conditions on the body's surface. In one-dimensional heat conduction, the energy conservation equation in cylindrical and spherical coordinate systems takes the following form:

$$\frac{1}{r^m}\frac{d}{dr}(r^m \dot{q}) = \dot{q}_v, \tag{A.3}$$

where m = 1 for a cylindrical wall and m = 2 for a spherical wall. The heat flux $\dot{q}$ is given by Fourier's law:

$$\dot{q} = -k\frac{\partial T}{\partial r}. \tag{A.4}$$

The temperature distribution is determined in a cylindrical and spherical wall under the following boundary conditions:

$$-k\frac{\partial T}{\partial r}|r = r_{in} = \dot{q}_{in}, \tag{A.5}$$

$$T|_{r=r_{out}} = T_{out}. \tag{A.6}$$

The heat flux $\dot{q}_{in}$ is specified at the inner surface of the cylindrical or spherical wall, and the temperature T_{out} is specified at the outer surface. The boundary problem (A.3)−(A.6) was solved for cylindrical and spherical walls using the above-mentioned approaches. In the first method, the temperature distribution was determined by applying the energy conservation equation (A.3), taking into account Fourier's law (A.4). In the second

method, the temperature distribution was determined by applying Fourier's law (A.4), taking into account the energy conservation equation (A.3).

A.1. Determination of the temperature distribution in a cylindrical and spherical wall using the first method

Substituting Fourier's law, given by Eq. (A.4), into Eq. (A.3) yields the following heat conduction equation:

$$\frac{1}{r^m}\frac{d}{dr}\left(r^m k\frac{\partial T}{\partial r}\right) = -\dot{q}_v. \tag{A.7}$$

Using Eq. (A.7), the temperature distributions in the cylindrical wall (m = 1) and spherical wall (m = 2) were determined separately:

- Cylindrical wall (m = 1):

  After multiplying Eq. (A.7) by r and dividing by k on both sides and integrating twice, the temperature distribution in the wall is obtained:

$$T = -\frac{1}{4}\frac{\dot{q}_v r^2}{k} + C\,ln\,r + C_1. \tag{A.8}$$

  Determining constants C and C_1 from boundary conditions (A.5) and (A.6), and then substituting them into the solution (A.8) gives:

$$T = T_{out} + \frac{1}{4}\frac{\dot{q}_v r_{out}^2}{k}\left(1 - \frac{r^2}{r_{out}^2}\right) + \\ + \left(\frac{\dot{q}_v r_{in}^2}{2k} - \frac{\dot{q}_{in} r_{in}}{k}\right) ln\frac{r}{r_{out}}. \tag{A.9}$$

- Spherical wall (m = 2):

  Multiplying Eq. (A.7) for m = 2 by r^2 and dividing by k and then integrating it twice gives:

$$T = -\frac{1}{6}\frac{\dot{q}_v r^2}{k} - \frac{C_3}{r} + C_4. \tag{A.10}$$

  After determining constants C_3 and C_4 from boundary conditions given by Eq. (A.5) and Eq. (A.6) and substituting them into Eq.(A.10), one gets:

$$T = T_{out} + \frac{1}{6}\frac{\dot{q}_v}{k}(r_{out}^2 - r^2) + \frac{1}{3}\frac{\dot{q}_v r_{in}^3}{k r_{out}}\left(\frac{1}{r_{out}} - \frac{1}{r}\right) + \\ + \frac{\dot{q}_{in} r_{in}^2}{k}\left(\frac{1}{r} - \frac{1}{r_{out}}\right). \tag{A.11}$$

Next, the temperature distributions in the cylindrical and spherical walls were determined using the second method.

A.2. Determination of the temperature distribution in a cylindrical and spherical wall using the second method

In the second method, the temperature distribution is determined using Fourier's law (A.4). First, the heat flux is determined from Eq. (A.3). After multiplying Eq. (A.3) by r^m and integrating it on both sides, one gets:

$$\dot{q} = \frac{\dot{q}_v}{m+1} r + \frac{C_5}{r^m}. \tag{A.12}$$

The boundary condition given by Eq. (A.6) can be written as:

$$\dot{q}|_{r=r_{in}} = \dot{q}_{in}. \tag{A.13}$$

Substituting Eq. (A.12) into Eq. (A.13) yields the constant C_5. Substituting the constant C_5 determined in this way into Eq. (A.12) gives:

$$\dot{q} = \frac{\dot{q}_v}{m+1} r + \left(\dot{q}_{in} r_{in}^m - \frac{\dot{q}_v}{m+1} r_{in}^{m+1}\right)\frac{1}{r^m}. \tag{A.14}$$

Substituting Eq. (A.14) into Eq. (A.4) representing Fourier's law, the following differential equation is obtained:

$$\frac{dT}{dr} = -\frac{\dot{q}_v}{(m+1)k} r - \left(\frac{\dot{q}_{in} r_{in}^m}{k} - \frac{\dot{q}_v}{(m+1)k} r_{in}^{m+1}\right)\frac{1}{r^m}. \tag{A.15}$$

Equation (A.15) will be used to determine the temperature distribution in the cylindrical and spherical walls:

- Cylindrical wall (m = 1):

  Integrating Eq. (A.15) for m = 1, results in:

$$T = -\frac{\dot{q}_v r^2}{4k} - \left(\frac{\dot{q}_{in} r_{in}}{k} - \frac{\dot{q}_v r_{in}^2}{2k}\right) ln\,r + C_6. \tag{A.16}$$

  By determining the constant C_6 from the boundary condition given by Eq. (A.6), Eq. (A.9) is obtained for calculating the temperature distribution in the cylindrical wall.

- Spherical wall (m = 2):

  Integrating Eq. (A.15) for m = 2, results in:

$$T = -\frac{\dot{q}_v r^2}{6k} + \left(\frac{\dot{q}_{in} r_{in}^2}{k} - \frac{\dot{q}_v r_{in}^3}{3k}\right)\frac{1}{r} + C_7. \tag{A.17}$$

  By determining the constant C_7 from the boundary condition given by Eq. (A.6), Eq. (A.11) is obtained for calculating the temperature distribution in the spherical wall.

Both methods then produce identical formulas for calculating the temperature distribution.